Physica Scripta

PAPER

Controllable sidebands of resonance fluorescence of a two-level system driven by bichromatic field

RECEIVED
21 February 2023

REVISED
19 March 2023

ACCEPTED FOR PUBLICATION
31 March 2023

PUBLISHED
11 April 2023

Yiying Yan[1,*], **Zhiguo Lü**[2], **JunYan Luo**[1] and **Hang Zheng**[2]

[1] Department of Physics, School of Science, Zhejiang University of Science and Technology, Hangzhou 310023, People's Republic of China
[2] Key Laboratory of Artificial Structures and Quantum Control (Ministry of Education), School of Physics and Astronomy, Shanghai Jiao Tong University, Shanghai 200240, People's Republic of China
[*] Author to whom any correspondence should be addressed.

E-mail: yiyingyan@zust.edu.cn **and** zglv@sjtu.edu.cn

Keywords: resonance fluorescence, Floquet theory, bichromatic field

Abstract

Strong polychromatic driving reshapes characteristics of the resonance fluorescence spectrum of a two-level system. Employing bichromatic driving feild with a low beat-frequency smaller than the emission rate of the system we demonstrate the exotic features of the fluorescence spectrum calculated by the numerical Floquet-Liouville approach and analytical method. It is found that fluorescence spectrum possesses two broadened sidebands in the place of the Rabi sidebands under certain conditions. Moreover, the heights and widths of the sidebands can be controlled by tuning the driving parameters. The properties of the spectrum is determined by the transitions between the Floquet states in a rotating frame. The broadened sidebands result from the quasi-continuous quasienergy spectrum which happens with steering the beat frequency lower. The present study provides insights into the Floquet engineering of the fluorescence spectral features with polychromatic excitation fields.

1. Introduction

Resonance fluorescence, radiating from quantum emitters driven by external fields, has been extensively studied theoretically and experimentally. For instance, this phenomenon has been studied in various emitters ranging from two-level atom [1–3] to multilevel ones [4–18] subjected to a variety of external fields ranging from monochromatic excitation fields to bi- and poly-chromatic ones [19–27]. Apart from different types of emitters and external fields, the investigations have also considered the influence of various environments with which the emitters interact on the resonance fluorescence,e.g. squeezed vacuum [28] and structured reservoir [29–31]. In addition to the spectroscopy, the study on the resonance fluorescence reveals the nonclassical features of the fluorescent light including squeezing [32–44], photon correlation [45, 46], quantum interference [11, 47–54], etc. It is directly relevant to the quantum technologies of indistinguishable single-photon source [55, 56] and generating nonclassical light [57–59].

In one of the simplest case, i.e. a two-level emitter driven by a monochromatic field, it turns out that the fluorescence spectrum has a nontrivial three-peaked structure, i.e. the celebrated Mollow triplet, in the strong driving regime where the Rabi frequency of the excitation field is much greater than the spontaneous emission rate of the emitter [1]. The Mollow triplet has been experimentally validated in the natural atoms [60, 61] as well as artificial atoms such as semiconductor quantum dots [62, 63] and superconducting circuits [64]. The origin of three-peaked structure can be understood by using the dressed-atom model [65, 66], where the emission lines arise from the transition between the dressed states of the atom and driving field.

When a two-level emitter is driven by a bichromatic field, the fluorescence spectrum exhibits even more complicated multipeaked structures [67–72]. The multipeaked structure strongly depends on the intensities and beat frequency of the bichromatic field. Particularly, the fluorescence spectrum has been studied in the cases of a bichromatic field with one strong and one weak component or with equally strong components. The theoretical predictions are recently validated in the context of semiconductor quantum dots [73, 74]. So far much more

attentions are paid to the high beat-frequency cases, namely, the beat frequency of the bichromatic field is greater than the emission rate of the system. However, the fluorescence spectrum in the case of low beat frequencies of bichromatic fields has not yet been fully explored.

In terms of the doubly dressed-atom model, Freedhoff and Ficek have considered a special case where a two-level system is dressed by two fields with equal frequencies and unequal intensities, corresponding to the zero beat-frequency limit of the bichromatic field, and have found that the energy spectrum of the doubly dressed atom consists of a ladder of doublet continua, which result in the broadened sidebands in the fluorescence spectrum [75]. Similar to the doubly dressed-atom model, the quasienergy spectrum of the bichromatically driven two-level system may become quasi-continuous. The bichromatically driven two-level system is unitarily equivalent to an effectively periodically driven system in the rotating frame when the rotating-wave approximation (RWA) is used [76]. Importantly, the effective driving frequency depends on the beat frequency of the bichromatic field. It is thus possible that the quasienergy ladder of the effective system can be quasi-continuous when the beat frequency is vanishingly small. This would result in significant modification of the resonance fluorescence spectrum from the Mollow triplet as well as the multipeaked structure. Therefore, it is worthwhile to reveal interesting spectral signatures associated with the quasi-continuous quasienergy spectrum in the low beat-frequency regimes.

In this work, we study the resonance fluorescence spectrum of a two-level system driven by a classical bichromatic field with a low beat frequency by using the Floquet-Liouville (FL) approach [77] and analytical method [78]. The FL numerical results and analytical results are found to be in agreement with each other in the strong driving regimes. We show that the quasienergy spectrum of the driven system can be quasi-continuous in the low beat-frequency regime. This leads to the formation of the broadened sidebands in the place of the Rabi sidebands in the fluorescence spectrum. When the Rabi frequencies of the bichromatic field are equal, it is revealed that exotic line shapes with broadened sidebands, which are vanishing in the high beat-frequency regime. When the bichromatic field consists of one strong and one weak component, the line shape somewhat resembles those found in [75]. The properties of the spectrum are explained as a consequence of the transitions between the semiclassical Floquet states.

The rest of the paper is organized as follows. In section 2, we introduce the model and theoretical methods, and present some analytical results. In section 3, we present the comparison between the numerical results and (semi-) analytical results, and illustrate the spectral features of the resonance fluorescence. In section 4, the conclusions are drawn.

2. Quasienergy spectrum and resonance fluorescence spectrum

With the RWA, the Hamiltonian of the bichromatically driven two-level system in free space is given by ($\hbar = 1$)

$$H_{\rm tot}(t) = H(t) + H_{\rm F} + H_{\rm I}, \tag{1}$$

$$H(t) = \frac{1}{2}\omega_0\sigma_z + \frac{\Omega}{2}[\sigma_-(e^{i\omega_1 t} + re^{i\omega_2 t}) + \sigma_+(e^{-i\omega_1 t} + re^{-i\omega_2 t})], \tag{2}$$

$$H_{\rm F} = \sum_k \omega_k b_k^\dagger b_k, \tag{3}$$

$$H_{\rm I} = \sum_k g_k(b_k\sigma_+ + b_k^\dagger\sigma_-). \tag{4}$$

Here, $H(t)$ describes that a two-level system with transition frequency ω_0 is coherently driven by a bichromatic field. Ω is the Rabi frequency of the first component of the bichromatic field, r is the ratio of the Rabi frequency of the second component of the bichromatic field to that of the first one. ω_1 and ω_2 are the frequencies of the bichromatic field, respectively. σ_μ ($\mu = x, y, z$) is the Pauli matrix and $\sigma_\pm = (\sigma_x \pm i\sigma_y)/2$. $H_{\rm F}$ is the free Hamiltonian of the vacuum radiation field described by a set of harmonic oscillator with frequency ω_k and creation (annihilation) operator $b_k^\dagger$ (b_k). $H_{\rm I}$ describes the interaction between the two-level system and the field, where g_k are coupling constants.

To proceed, the Hamiltonian is transformed into a frame rotating at the average frequency $\overline{\omega} = (\omega_1 + \omega_2)/2$, yielding

$$\begin{aligned}\tilde{H}_{\rm tot}(t) &= R(t)[H_{\rm tot}(t) - i\partial_t]R^\dagger(t)\\ &= \tilde{H}(t) + H_{\rm F} + H_{\rm I},\end{aligned} \tag{5}$$

$$\tilde{H}(t) = \frac{1}{2}\Xi\sigma_z + \frac{\Omega}{2}[\sigma_-(e^{-i\omega_b t} + re^{i\omega_b t}) + \sigma_+(e^{i\omega_b t} + re^{-i\omega_b t})], \tag{6}$$

where $R(t) = \exp[i\bar{\omega}(\frac{\sigma_z}{2} + \sum_k b_k^\dagger b_k)t]$, $\Xi = \omega_0 - \overline{\omega}$ is the average detuning, and $\omega_b = (\omega_2 - \omega_1)/2$ is the half of the beat frequency of the bichromatic field. Without loss of generality, we assume $\omega_b > 0$ throughout this

work. In the rotating frame, one notes that $\tilde{H}(t)$ is periodic in time with a periodicity $T = 2\pi/\omega_b$, which allows us to use the Floquet theory [79].

Using $\tilde{H}(t) + H_{\rm F}$ and $H_{\rm I}$ as the free and perturbation Hamiltonian respectively, one is able to derive the master equation for describing the time evolution of the driven two-level system with the Born-Markov approximation [66]. Assuming $\Omega \ll \omega_0$, the master equation is found to be a standard Lindblad form in the rotating frame,

$$\frac{\mathrm{d}}{\mathrm{d}t}\rho(t) = -\mathrm{i}[\tilde{H}(t),\, \rho(t)] - \frac{\kappa}{2}[\sigma_+\sigma_-\rho(t) + \rho(t)\sigma_+\sigma_- - 2\sigma_-\rho(t)\sigma_+], \tag{7}$$

where $\rho(t)$ is the density matrix of the two-level system, and κ is the spontaneous decay rate. The detailed derivation of the master equation can be found in the appendix A. In the following, we first discuss the Floquet quasienergy spectrum associated with $\tilde{H}(t)$ and then use two different methods based on the Floquet theory to solve the master equation, and finally derive the resonance fluorescence spectrum which is relevant to the quasienergy spectrum of the driven system.

2.1. Quasi-continuous Floquet quasienergy spectrum

We discuss the quasi-continuous quasienergy spectrum of the effective system $\tilde{H}(t)$. To elucidate this, we first consider the dissipationless driven system which satisfies the time-dependent Schrödinger equation,

$$\mathrm{i}\frac{\mathrm{d}}{\mathrm{d}t}|\psi(t)\rangle = \tilde{H}(t)|\psi(t)\rangle. \tag{8}$$

According to the Floquet theory [79], the solution to the time-dependent Schrödinger equation takes the form $|\psi_\alpha(t)\rangle = \exp(-\mathrm{i}\varepsilon_\alpha t)|u_\alpha(t)\rangle$, where the index $\alpha = \pm$ is used to distinguish the linearly independent solutions, $|u_\alpha(t)\rangle = |u_\alpha(t+T)\rangle$ is the Floquet state, and ε_α is the real-valued quasienergy. Substituting the formal solution into equation (8), we find

$$[\tilde{H}(t) - \mathrm{i}\partial_t]|u_\alpha(t)\rangle = \varepsilon_\alpha|u_\alpha(t)\rangle. \tag{9}$$

On solving this equation, one finds the Floquet states and quasienergies. If $|u_\alpha(t)\rangle$ is a solution with the quasienergy ε_α, $|u_{\alpha,l}(t)\rangle = \exp(\mathrm{i}l\omega_b t)|u_\alpha(t)\rangle$ is also a solution with the shifted quasienergy $\varepsilon_{\alpha,l} = \varepsilon_\alpha + l\omega_b$. Typically, ε_α is referred to as the quasienergy in the first Brillouin zone $[-\omega_b/2, \omega_b/2)$. Thus, it is not difficult to imagine that the quasienergy spectrum may become quasi-continuous as $\omega_b \to 0$.

To be concrete, let us consider an exactly solvable case $\Xi = 0$ and $r = 1$. In this case, the Floquet state and corresponding quasienergy can be found as follows:

$$|u_{\pm,l}(t)\rangle = \exp\left[\mathrm{i}l\omega_b t \mp \mathrm{i}\frac{\Omega}{\omega_b}\sin(\omega_b t)\right]|\pm\rangle, \tag{10}$$

$$\varepsilon_{\pm,l} = l\omega_b, \tag{11}$$

where $|\pm\rangle$ are the eigenstates of σ_x with eigenvalues ± 1. Clearly, the quasienergy spectrum becomes quasi-continuous with a vanishingly small ω_b. In addition, one finds that for a fixed l, the quasienergies are degenerate. When $\Xi \neq 0$ or $r \neq 1$, the degeneracy of the quasienergies can be lifted and equation (9) may not be exactly solved by analytical methods. Nevertheless, it is feasible to numerically solve equation (9) by using the Fourier expansion, which converts the differential equations into a linear algebra eigenvalue problem with an infinite Floquet Hamiltonian [79, 80]. The Floquet Hamiltonian can be numerically diagonalized with an appropriate truncation. In the following we show that the quasi-continuous quasienergy spectrum is manifested in the formation of the broadened sideband in resonance fluorescence spectrum.

2.2. Resonance fluorescence spectrum

We calculate the steady-state resonance fluorescence spectrum, which is the Fourier transform of the first-order correlation function [81]

$$S(\Delta) = \mathrm{Re}\int_0^\infty g(\tau)\mathrm{e}^{-\mathrm{i}\Delta\tau}d\tau, \tag{12}$$

$$g(\tau) = \frac{1}{T}\int_0^T \lim_{t'\to\infty}\langle\sigma_+(t'+\tau)\sigma_-(t')\rangle\, dt', \tag{13}$$

where $g(\tau)$ is the time-averaged first-order two-time correlation function and $\Delta = \omega - \varpi$ is the detuning from the frequency of the fluorescent photon to the average frequency. In this work, we use two different methods to calculate the spectrum. The first method is the Floquet-Liouville (FL) approach, which is used to solve the master equation directly [77] and to derive the two-time correlation function associated with the quantum regression theorem [81]. This treatment is numerically exact. The details of the FL approach for the present model is presented in the appendix B. The other method is to solve the master equation in the Floquet picture with the aid

of the secular approximation [78], which allows us to derive a physically transparent spectral expression and provides insights into the spectral features.

We state briefly the analytical treatment. First, we rewrite the master equation in terms of the Floquet states $|u_\alpha(t)\rangle$ and invoke the secular approximation [78], yielding

$$\frac{\mathrm{d}}{\mathrm{d}t}\rho_{++}(t) = -\Gamma_{\mathrm{rel}}\rho_{++}(t) + \Gamma_0, \tag{14}$$

$$\frac{\mathrm{d}}{\mathrm{d}t}\rho_{+-}(t) = -(\mathrm{i}\Delta\varepsilon_{+-} + \Gamma_{\mathrm{deph}})\rho_{+-}(t), \tag{15}$$

where $\rho_{\alpha\beta}(t) = \langle u_\alpha(t)|\rho(t)|u_\beta(t)\rangle$ is the density matrix element in the Floquet picture, $\Delta\varepsilon_{+-} = \varepsilon_+ - \varepsilon_-$ is the quasienergy difference. Γ_{rel} and Γ_{deph} are the relaxation and dephasing rate of the Floquet states, respectively, and Γ_0 is an inhomogeneous term determining the steady state of the Floquet states. The explicit form of the rates are given by

$$\Gamma_0 = \kappa \sum_{l=-\infty}^{\infty} |x^{(+)}_{-+,l}|^2, \tag{16}$$

$$\Gamma_{\mathrm{rel}} = \kappa \sum_{l=-\infty}^{\infty} (|x^{(+)}_{+-,l}|^2 + |x^{(+)}_{-+,l}|^2), \tag{17}$$

$$\Gamma_{\mathrm{deph}} = \frac{\kappa}{2} \sum_{l=-\infty}^{\infty} (|x^{(+)}_{+-,l}|^2 + |x^{(+)}_{-+,l}|^2 + 4|x^{(+)}_{++,l}|^2), \tag{18}$$

where

$$x^{(\pm)}_{\alpha\beta,l} = \frac{1}{T}\int_0^T \langle u_\alpha(t)|\sigma_\pm|u_\beta(t)\rangle\, \mathrm{e}^{-\mathrm{i}l\omega_b t}\mathrm{d}t \tag{19}$$

is the time-averaged transition matrix elements between Floquet states. Second, the solution of the equations above are obtained

$$\rho_{++}(t) = \rho_{++}(0)\mathrm{e}^{-\Gamma_{\mathrm{rel}}t} + \rho^{\mathrm{ss}}_{++}(1 - \mathrm{e}^{-\Gamma_{\mathrm{rel}}t}), \tag{20}$$

$$\rho_{+-}(t) = \rho_{+-}(0)\mathrm{e}^{-(\mathrm{i}\Delta\varepsilon_{+-}+\Gamma_{\mathrm{deph}})t}, \tag{21}$$

where $\rho^{\mathrm{ss}}_{++} = \Gamma_0/\Gamma_{\mathrm{rel}}$ is the steady Floquet state population. Finally, by using the quantum regression theorem [81] and the above solutions, we derive the formal spectrum [78]:

$$\begin{aligned} S(\Delta) = \sum_{l=-\infty}^{\infty} \Bigg\{ & \pi|x^{(+)}_{++,l}|^2(\rho^{\mathrm{ss}}_{++} - \rho^{ss}_{--})^2\delta(\Delta - l\omega_b) \\ & + 4|x^{(+)}_{++,l}|^2\rho^{\mathrm{ss}}_{++}\rho^{\mathrm{ss}}_{--}\frac{\Gamma_{\mathrm{rel}}}{\Gamma^2_{\mathrm{rel}} + (\Delta - l\omega_b)^2} \\ & + |x^{(+)}_{+-,l}|^2\rho^{\mathrm{ss}}_{++}\frac{\Gamma_{\mathrm{deph}}}{\Gamma^2_{\mathrm{deph}} + (\Delta - l\omega_b - \Delta\varepsilon_{+-})^2}, \\ & + |x^{(+)}_{-+,l}|^2\rho^{\mathrm{ss}}_{--}\frac{\Gamma_{\mathrm{deph}}}{\Gamma^2_{\mathrm{deph}} + (\Delta - l\omega_b + \Delta\varepsilon_{+-})^2}\Bigg\}, \end{aligned} \tag{22}$$

where the Dirac-delta functions are the coherent components of the spectrum while the Lorentzian ones are the incoherent components. The basic ingredients such as the linewidths, peak positions, and weights in the above expression can be calculated with the Floquet states $|u_\alpha(t)\rangle$ and quasienergies ε_α of the driven system. Therefore, if the Floquet states and the quasienergies are already known, the spectrum is completely determined. We should emphasis that the validity of this formal spectrum just depends on the validity of the secular approximation used in the Floquet picture when the Floquet states and quasienergies are exact. The secular approximation is justified in the strong driving regime. In general, it is difficult to analytically obtain the exact quasienergies and Floquet states in most cases. Nevertheless, they can be computed numerically exactly by the numerical diagonalization of the Floquet Hamiltonian [79, 80].

Provided the analytical Floquet states and quasienergies are known, the analytical spectrum can be derived by equation (22). Considering an important case, i.e. $\Xi = 0$ and $r = 1$, we obtain a very simple analytical spectrum to illustrate the features of the spectrum. By equation (10), we derive the explicit form of $x^{(+)}_{\alpha\beta,l}$:

$$x^{(+)}_{++,l} = -x^{(+)}_{--,l} = \frac{1}{2}\delta_{l,0}, \tag{23}$$

$$x^{(+)}_{+-,l} = -\frac{1}{2}J_l\left(\frac{2\Omega}{\omega_b}\right), \tag{24}$$

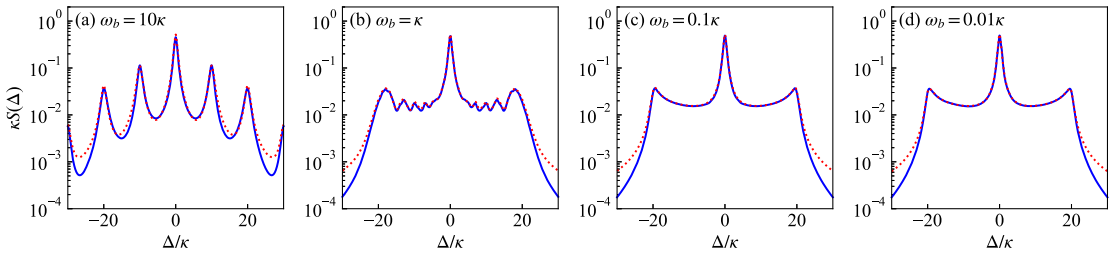

Figure 1. Incoherent resonance fluorescence spectra calculated by the FL approach (solid lines) and equation (26) (dotted lines) for $\Omega = 10\kappa$, $\Xi = 0$, $r = 1$, and four values of ω_b.

$$x^{(+)}_{-+,l} = \frac{1}{2} J_{-l}\left(\frac{2\Omega}{\omega_b}\right), \tag{25}$$

where $\delta_{l,l'}$ is the Kronecker-delta function and $J_l(\cdot)$ is the Bessel function of the first kind with integer order l. Using these elements, equation (11), and the identity $\sum_{l=-\infty}^{\infty} J_l^2(z) = 1$, we readily derive an analytical spectrum as follows:

$$S(\Delta) = \frac{1}{4}\frac{\frac{\kappa}{2}}{\frac{1}{4}\kappa^2 + \Delta^2} + \frac{1}{4}\sum_{l=-\infty}^{\infty} J_l^2\left(\frac{2\Omega}{\omega_b}\right)\frac{\frac{3}{4}\kappa}{\frac{9}{16}\kappa^2 + (\Delta - l\omega_b)^2}, \tag{26}$$

where the first term representing the central line is the same as that of the Mollow triplet [1], and the terms in the summation are corresponding to the sidebands ($l \neq 0$) and the modification to the central line ($l = 0$). Besides, one finds that the Dirac-delta functions vanish because $\rho^{ss}_{++} = \rho^{ss}_{--} = 1/2$, which is actually a consequence of the secular approximation and can be justified in the strong driving case. Equation (26) provides the manifest insights into the spectral features in the case of $\Xi = 0$ and $r = 1$. First, the spectrum is found to be symmetric about $\Delta = 0$. The symmetry of the spectrum can be attributed to the generalized parity of the driven system [82–84]. The generalized parity appears only when $\Xi = 0$ and $r = 1$ and is broken otherwise. Second, there occur well separated multiple sidebands or broadened sidebands which depends on the value of ω_b. If $\omega_b \gg \kappa$, the sidebands become well separated and a multipeaked spectrum can be expected, which has been theoretically illustrated and experimentally verified in the previous works [70–74]. However, if the beat frequency is low enough, i.e. $\omega_b \ll \kappa$, a great number of Rabi sidebands are generated and not obviously separated from their neighbors. A broadened sideband comes into being.

When $\Xi = 0$ and $r \neq 1$ or $\Xi \neq 0$ and $r \neq 0$, we use the numerical diagonalization of the Floquet Hamiltonian to compute the Floquet states and quasienergies which is not available by the analytical method. Then, we also use equation (22) to compute the spectrum. Hereafter, the obtained spectrum is referred to as the semianalytical result. In contrast to the case of $\Xi = 0$ and $r = 1$, the spectrum is expected to be asymmetric due to the fact that the generalized parity of $\tilde{H}(t)$ is broken when $\Xi \neq 0$ and/or $r \neq 1$ [82]. On the other hand, similar to the previous case, the Rabi sidebands may be replaced with broadened sidebands when $\omega_b \ll \kappa$.

3. Numerical results and discussions

In this section, we calculate the resonance fluorescence spectrum in the low beat-frequency regime by using both the numerically exact FL approach and the analytical method. Then, we discuss the influence of the driving parameters on the spectral features of the incoherent components of the spectrum .

To begin with, we illustrate how the structure of the fluorescence spectrum evolves with the variation of the beat frequency. Figure 1(a)- 1(d) display the incoherent components of the fluorescence spectra calculated by the FL approach (solid lines) and equation (26) (dotted lines) for $\Omega = 10\kappa$, $\Xi = 0$, $r = 1$, and four values of ω_b arranged in a descending order. The numerically exact results agree well with those obtained by equation (26), indicating the validity of the latter. It is clear to see that the spectrum possesses a multipeak structure when the beat frequency is greater than or comparable with the emission rate [see figure 1(a) and 1(b)]. Meanwhile, the multipeak feature comes to disappear with the decrease of ω_b. When the beat frequency is much smaller than the emission rate, the spectrum exhibits two broadened sidebands. Moreover, it turns out that the spectrum is weakly dependent on ω_b when ω_b is low enough.

To further illustrate the dependence of the intensities of the central line and the sidebands on the beat frequency, we use equation (26) to calculate the intensities of spectral components $S(\Delta)$ at $\Delta = 0, \Omega, 1.5\Omega, 2\Omega$ as a function of beat frequency ω_b for $\Xi = 0, \Omega = 10\kappa$, and $r = 1$, where $S(0)$ characterizes the central line and $\{S(\Delta)|\Delta = \Omega, 1.5\Omega, 2\Omega\}$ is used to characterize the sideband. The behaviors of these spectral components are

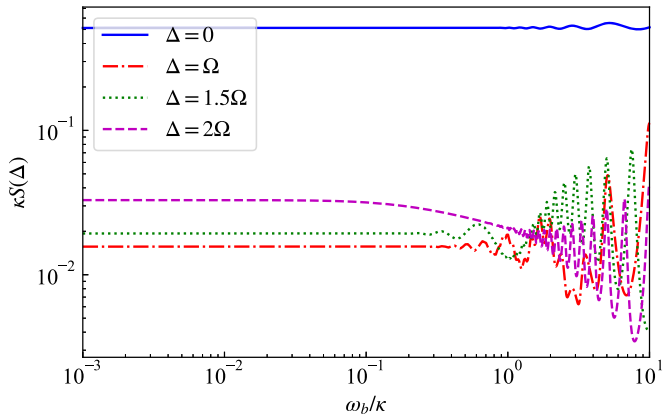

Figure 2. Intensities of spectral components at $\Delta = 0, \Omega, 1.5\Omega, 2\Omega$ as a function of beat frequency ω_b calculated from equation (26) for $\Xi = 0, \Omega = 10\kappa$, and $r = 1$.

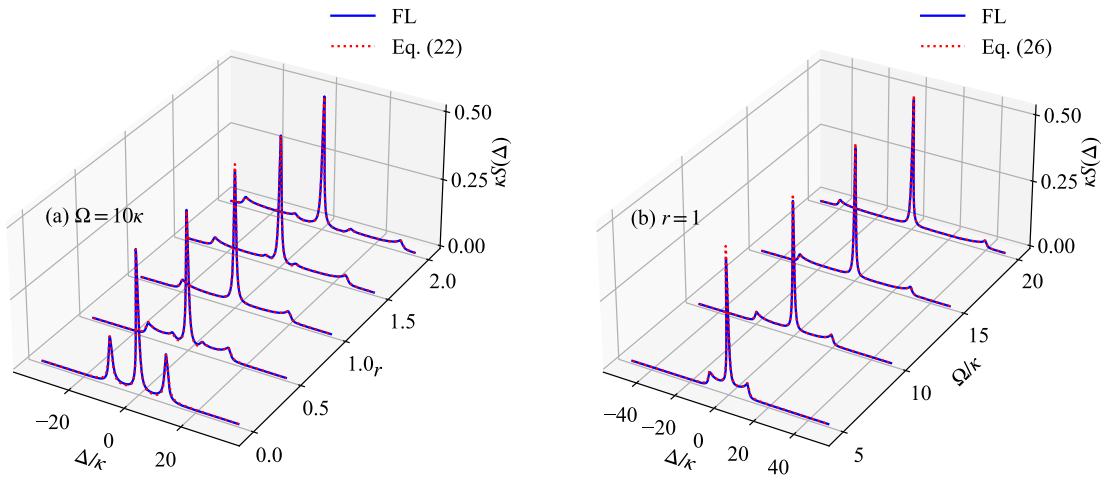

Figure 3. (a) Incoherent resonance fluorescence spectra calculated by the FL approach and equation (22) for $\Omega = 10\kappa$ and various values of r. (b) Incoherent resonance fluorescence spectrum calculated by the FL approach and equation (26) for $r = 1$ and various values of Ω. The other parameters are set as $\Xi = 0$ and $\omega_b = 0.1\kappa$.

shown in figure 2. When $\omega_b > \kappa$, the spectral components of the central line and the sidebands exhibit oscillatory behaviors as ω_b increases, owing to the property of the Bessel functions. On the contrary, when $\omega_b < 0.1\kappa$, the oscillations in the central line and sidebands disappear, and the spectrum hardly changes as the beat frequency decreases below a threshold value, attributed to the asymptotic behavior of the Bessel functions.

Next, we show how the broadened sideband changes with the variation of r when $\omega_b = 0.1\kappa$ and the other parameters are fixed. In figure 3(a), we show the incoherent components of the resonance fluorescence spectrum $S(\Delta)$ as a function of Δ calculated by the FL approach and equation (22) for $\Xi = 0$, $\omega_b = 0.1\kappa$, $\Omega = 10\kappa$, and various values of r ranging from 0 to 2. When $r = 0$, the spectrum is the standard Mollow triplet. As r increases, the central line is almost unchanged while the Rabi sidebands are replaced with the broadened sidebands. Interestingly, when r is much smaller or greater than 1, there are two peaks in each sideband. However, when $r = 1$, there is only one peak in a sideband. The spectra in the case of $r \neq 1$ somewhat resemble those from a two-level system driven by two fields with equal frequency, where one field is strong and the other is weak [75]. Nevertheless, we should point out that the spectra in the case of $r \neq 1$ are slightly asymmetric while the spectra in the latter case is exactly symmetric. In addition, we note that the numerical FL results and semianalytical results are in agreement with each other.

To see how the variation of the Rabi frequency influences the spectral profile, in figure 3(b), we show the incoherent components of the resonance fluorescence spectrum $S(\Delta)$ as a function of Δ for $\Xi = 0$, $\omega_b = 0.1\kappa$, $r = 1$, for different values of the Rabi frequency Ω. With the increase of Ω, the sidebands become broadening while their heights decrease, indicating that the height and width can be tuned by the driving strength. We have performed the numerical calculation for the case of $r \neq 1$. It turns out that the variation of the sidebands with the

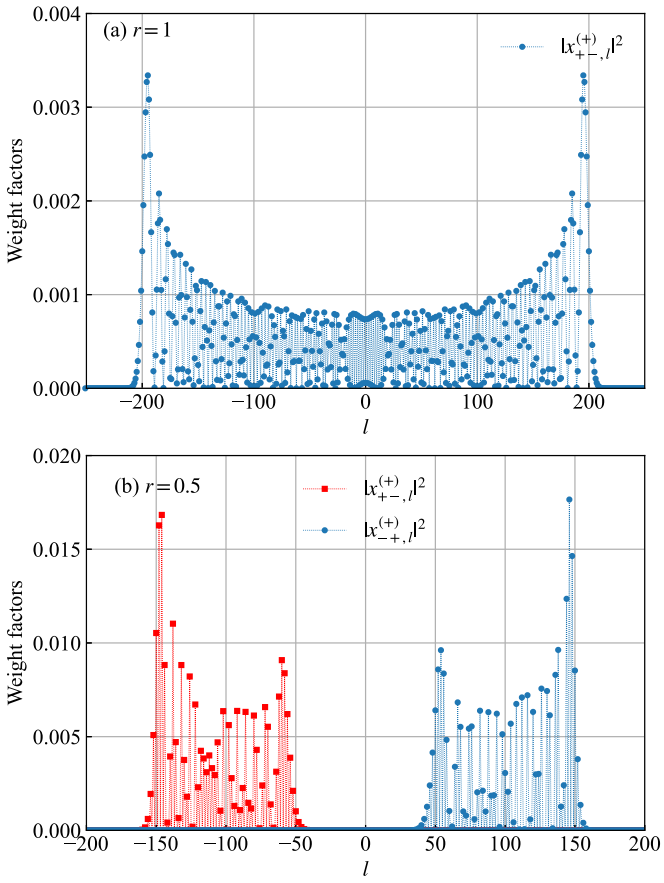

Figure 4. Weight factors $|x^{(+)}_{+-,l}|^2$ and $|x^{(+)}_{-+,l}|^2$ versus the index l for $\Xi = 0, \Omega = 10\kappa, \omega_b = 0.1\kappa$, and two values of r. In panel (a) only $|x^{(+)}_{+-,l}|^2$ is presented because $|x^{(+)}_{-+,l}|^2 = |x^{(+)}_{+-,l}|^2 = J_l^2(2\Omega/\omega_b)/4$. In panel (b) the weight factors are computed from the numerical diagonalization of the Floquet Hamiltonian.

increase of Ω in the case of $r \neq 1$ is similar to that in the case of $r = 1$. The properties of the sidebands can be completely attributed to the weight factors $|x^{(+)}_{+-,l}|^2$ and $|x^{(+)}_{-+,l}|^2$.

To clarify the observed properties of the sidebands, we carry out numerical calculations concerning on the weight factors $|x^{(+)}_{+-,l}|^2$ and $|x^{(+)}_{-+,l}|^2$ as a function of the index l. Figure 4 displays the results for $\Xi = 0, \Omega = 10\kappa$, $\omega_b = 0.1\kappa$, and two values of r. Figure 4 illustrates that it is the envelope of the weight factors that results in the profiles of the sidebands. Let us first focus on the case of $r = 1$, i.e. the bichromatic field consists of equally intense components. We have $|x^{(+)}_{+-,l}|^2 = |x^{(+)}_{-+,l}|^2 = J_l^2(2\Omega/\omega_b)/4$, i.e. the weight factors are identical for any l. Moreover, the weight factors are symmetric about $l = 0$ and there are two maxima near $l = \pm 200$. Such maxima in turn result in two peaks located near at $\Delta = l\omega_b$ in the spectrum. On the other hand, since $\sum_{l=-\infty}^{+\infty} J_l^2(2\Omega/\omega_b) = 1$ regardless of Ω, the integrated intensity of sidebands (the area under the sideband curve) remains fixed in strong driving regime. The increase in Ω can lead to the decrease in magnitudes of the Bessel functions $J_l(2\Omega/\omega_b)$ for a fixed small ω_b (due to the asymptotic behaviors of the Bessel functions with $2\Omega/\omega_b \gg 1$). Therefore, the width of the sidebands should increase to keep the integrated intensity of the sidebands invariable. This explains the change of the width and height of the sidebands as a function of Ω observed in figure 3(b).

Let us analyze the properties of the weight factors for r=0.5, i.e. the bichromatic field consists of two components with unequal intensities. First of all, from figure 4(b), we see that $|x^{(+)}_{+-,l}|^2$ and $|x^{(+)}_{-+,l}|^2$ are not identical to each other when $r \neq 1$. Particularly, $|x^{(+)}_{+-,l}|^2$ is generally unequal to $|x_{-+,-l}|^2$, which leads to the asymmetry of the spectrum. Secondly, the nonzero elements of $|x^{(+)}_{+-,l}|^2$ and those of $|x^{(+)}_{-+,l}|^2$ are well separated. Thirdly, there are two local maxima in each weight factors. For $|x^{(+)}_{+-,l}|^2$ and $|x^{(+)}_{-+,l}|^2$, their local maxima appear around $l = -100$ and $l = +100$, respectively. These properties result in separated red and blue sideband continua and each continuum consists of two peaks located near at $\Delta = l\omega_b$ when $r < 1$.

We examine the influence of the average detuning Ξ on the fluorescence spectrum. Figure 5 shows the incoherent fluorescence spectra for $\Omega = 10\kappa, \omega_b = 0.1\kappa, r = 1$, and various values of Ξ. As the magnitude of Ξ increases, the height of the central line decreases. This simply reflects the fact that the bichromatic field is tuned to be off-resonant with the two-level system for a large $|\Xi|$ and a small ω_b. In contrast, the sidebands are slightly

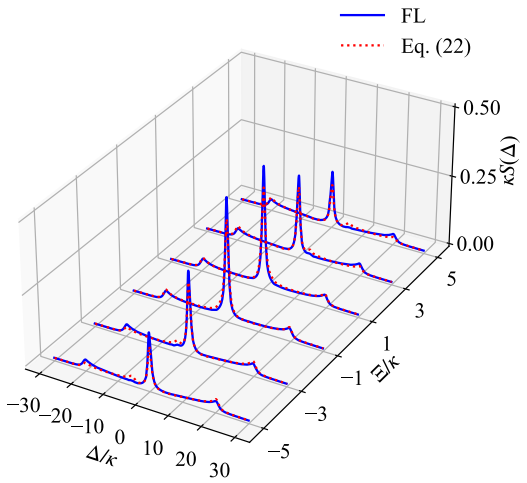

Figure 5. Incoherent resonance fluorescence spectra calculated by the FL approach and equation (22) with the numerical diagonalization of the Floquet Hamiltonian for $\Omega = 10\kappa, \omega_b = 0.1\kappa, r = 1$, and the various values of the average detuning Ξ.

modified with the variation of the average detuning. The spectra are asymmetric with a finite average detuning. In addition, although the semianalytical treatment is found to produce qualitatively correct results, its predictions quantitatively deviate from the numerically exact FL results for a finite average detuning, indicating that the secular approximation is not well justified in such cases.

The present results demonstrate that there are broadened sidebands in the place of the typical Rabi sidebands when the beat frequency is sufficiently small. The presented line shapes are different from the standard Mollow triplet from a monochromatically driven two-level system, and also the multipeaked spectrum from a bichromatically driven two-level system with a high beat frequency ($\omega_b \gg \kappa$). On the other hand, the present results validate the semianalytical and analytical treatment. This allows us to use the physical picture behind the analytical treatment to provide a simple physical interpretation of the properties of the spectrum. The physical picture can be established as follows. An emission line can be viewed as a consequence of the transition between the Floquet states [78, 85]. For instance, a transition from $|u_{+,l}(t)\rangle$ to $|u_{-,0}(t)\rangle$ results in the emission line at $\Delta = \Delta\varepsilon_{+-} + l\omega_b$, which is just the quasienergy spacing of the two Floquet states. The weight factor $|x^{(+)}_{+-,l}|^2$ quantifies the contribution of such a transition to the spectrum. With this simple physical picture, it is obvious to see that a great number of the allowed transitions of that type can lead to a great number of emission lines. Moreover, if the quasienergy spectrum is quasi-continuous, the positions of such emission lines become dense enough to form the broadened sideband continuum. From the present analysis, we can see that the broadened sidebands are the manifestation of the quasi-continuous quasienergy spectrum.

4. Conclusions

In summary, we have studied the resonance fluorescence spectrum of a two-level system driven by a bichromatic field with low beat frequency by using the numerically exact FL approach and analytical method. The results of the two approaches are found to be consistent with each other in the strong driving regimes. We have illustrated that when the Rabi frequencies of the bichromatic field are equal and the average detuning vanishes, the spectrum is symmetric and possesses two broadened sidebands in the place of the Rabi sidebands, which is different from line shapes in the high beat-frequency regime. The heights and widths of the sidebands can be controlled by tuning driving parameters. When the Rabi frequencies of the bichromatic field are unequal, the spectrum is asymmetric regardless of the average detuning and the spectral profiles are somewhat resemble those from a two-level system driven by two fields with equal frequencies and unequal intensities [75]. The properties of the spectrum can be understood as the consequence of the transitions between the Floquet states. The broadened sidebands are relevant to the quasi-continous quasienergy spectrum occurring in the low beat-frequency regimes. The present results provide insights into the fluorescent spectral features of a bichromatically driven two-level system in the low beat-frequency regime.

Acknowledgments

Support from the National Natural Science Foundation of China (Grants No. 12005188, No. 11774226, and No. 11774311) is gratefully acknowledged.

Data availability statement

The data that support the findings of this study are openly available at [86].

Appendix A. Derivation of the master equation

In the interaction picture governed by the free Hamiltonian $H_0(t) = \tilde{H}(t) + H_{\rm F}$, the density matrix $\rho^{\rm I}_{\rm tot}(t)$ of the driven two-level system and the radiation reservoir satisfies the Liouville-von Neumann equation

$$\frac{\rm d}{{\rm d}t}\rho^{\rm I}_{\rm tot}(t) = -{\rm i}[H_{\rm I}(t),\, \rho^{\rm I}_{\rm tot}(t)], \tag{A.1}$$

where

$$H_{\rm I}(t) = \sum_k g_k[b_k\sigma_+(t)e^{-{\rm i}\omega_k t} + b_k^\dagger\sigma_-(t)e^{{\rm i}\omega_k t}]. \tag{A.2}$$

The operators $\sigma_\pm(t)$ are given by

$$\sigma_\pm(t) = \tilde{U}^\dagger(t)\sigma_\pm\tilde{U}(t), \tag{A.3}$$

where

$$\begin{aligned}\tilde{U}(t) &= \mathcal{T}\exp\left[-{\rm i}\int_0^t \tilde{H}(\tau){\rm d}\tau\right]\\ &= \sum_{\alpha=\pm} |u_\alpha(t)\rangle\langle u_\alpha(0)|e^{-{\rm i}\varepsilon_\alpha t},\end{aligned} \tag{A.4}$$

is the time evolution operator of the driven system and $\mathcal{T}$ is the time-ordering operator. The second line follows from the Floquet theory [79] and $|u_\alpha(t)\rangle$ and ε_α are the Floquet state and quasienergy for the driven system, respectively. The equation can be formally integrated and yields

$$\rho^{\rm I}_{\rm tot}(t) = -{\rm i}\int_0^t [H_{\rm I}(\tau),\, \rho^{\rm I}_{\rm tot}(\tau)]{\rm d}\tau. \tag{A.5}$$

Substituting this formal solution into equation (A.1) and taking the partial trace over the degrees of freedom of the radiation field, one arrives at

$$\frac{\rm d}{{\rm d}t}\rho^{\rm I}(t) = -{\rm Tr}_{\rm F}\int_0^t [H_{\rm I}(t),\, [H_{\rm I}(\tau),\, \rho^{\rm I}_{\rm tot}(\tau)]]{\rm d}\tau, \tag{A.6}$$

where $\rho^{\rm I}(t) = {\rm Tr}_{\rm F}\rho^{\rm I}_{\rm tot}(t)$ and we have assumed a factorized initial state $\rho^{\rm I}_{\rm tot}(0) = \rho^{\rm I}(0)\otimes\rho_{{\rm F},vac}$ with $\rho_{{\rm F},vac}$ the vacuum state of the radiation field.

To proceed, we use the Born-Markov approximation, that is, $H_{\rm I}(\tau)$ and $\rho^{\rm I}_{\rm tot}(\tau)$ in the integral are replaced by $H_{\rm I}(t-\tau)$ and $\rho^{\rm I}(t)\otimes\rho_{{\rm F},vac}$ respectively, and the upper limit of the integral is extended to infinity. These approximations are justified in the weak coupling regime, where the correlation time of the bath is short [66]. Under the Born-Markov approximation, the master equation at zero temperature is given by

$$\frac{\rm d}{{\rm d}t}\rho^{\rm I}(t) = -{\rm Tr}_{\rm F}\int_0^\infty [H_{\rm I}(t),\, [H_{\rm I}(t-\tau),\, \rho^{\rm I}(\tau)\rho_{{\rm F},vac}]]{\rm d}\tau. \tag{A.7}$$

The partial trace and integral can be taken explicitly as follows:

$$\begin{aligned}[{\rm I}] &= \int_0^\infty {\rm d}\tau\, {\rm Tr}_{\rm F}[H_{\rm I}(t)H_{\rm I}(t-\tau)\rho^{\rm I}(\tau)\rho_{{\rm F},vac}]\\ &= \int_0^\infty \sum_k g_k^2 e^{-{\rm i}\omega_k\tau}\sigma_+(t)\sigma_-(t-\tau)\rho^{\rm I}(t){\rm d}\tau\\ &= \int_0^\infty \sum_k g_k^2 e^{-{\rm i}\omega_k\tau}\sigma_+(t)\sum_{\alpha,\beta,n}|u_\alpha(0)\rangle x^{(-)}_{\alpha\beta,n}\langle u_\beta(0)|e^{{\rm i}(\varepsilon_\alpha-\varepsilon_\beta+n\omega_b)(t-\tau)}\rho^{\rm I}(t){\rm d}\tau\\ &= \int_0^\infty \sum_k g_k^2 e^{-{\rm i}(\omega_k+\varepsilon_\alpha-\varepsilon_\beta+n\omega_b)\tau}\sigma_+(t)\sum_{\alpha,\beta,n}|u_\alpha(0)\rangle x^{(-)}_{\alpha\beta,n}\langle u_\beta(0)|e^{{\rm i}(\varepsilon_\alpha-\varepsilon_\beta+n\omega_b)t}\rho^{\rm I}(t){\rm d}\tau\\ &\approx \frac{\kappa}{2}\sigma_+(t)\sigma_-(t)\rho^{\rm I}(t),\end{aligned} \tag{A.8}$$

where we have used the expansion follows from the Floquet theory: $\sigma_-(t-\tau)=\sum_{\alpha,\beta,n}|u_\alpha(0)\rangle x^{(-)}_{\alpha\beta,n}\langle u_\beta(0)|e^{i(\varepsilon_\alpha-\varepsilon_\beta+n\omega_b)(t-\tau)}$ with $x^{(-)}_{\alpha\beta,n}$ defined in equation (19). In addition we have approximated the integral by

$$\int_0^\infty \sum_k g_k^2 e^{-i(\omega_k+\varepsilon_\alpha-\varepsilon_\beta+n\omega_b)\tau}d\tau \approx \frac{\kappa}{2}, \tag{A.9}$$

which is justified when $\Omega \ll \omega_0$. The other terms in the right-hand side of equation (A.7) can be evaluated similarly as [I]. Finally, one transforms the obtained master equation back into the rotating frame and derives equation (7) in the main text.

Appendix B. Floquet-Liouville approach

To solve the master equation, we first rewrite it in a matrix form,

$$i\frac{d}{dt}\vec{\sigma}(t)=M(t)\vec{\sigma}(t)+\vec{b}, \tag{B.1}$$

where

$$\vec{\sigma}(t)=\left(\langle\sigma_+(t)\rangle \;\; \langle\sigma_-(t)\rangle \;\; \langle\sigma_z(t)\rangle\right)^{\mathrm{T}}, \tag{B.2}$$

and

$$\langle\sigma_\mu(t)\rangle=\mathrm{Tr}[\sigma_\mu\rho(t)] \quad (\mu=\pm,z) \tag{B.3}$$

is the single-time expectation value. The inhomogeneous vector is given by

$$\vec{b}=i(0 \;\; 0 \;\; -\kappa)^{\mathrm{T}}. \tag{B.4}$$

The coefficient matrix reads

$$\begin{aligned} M(t)&=\begin{pmatrix} -\Xi-i\frac{\kappa}{2} & 0 & \frac{\Omega}{2}(e^{-i\omega_b t}+re^{i\omega_b t}) \\ 0 & \Xi-i\frac{\kappa}{2} & -\frac{\Omega}{2}(e^{i\omega_b t}+re^{-i\omega_b t}) \\ \Omega(e^{-i\omega_b t}+re^{i\omega_b t}) & -\Omega(e^{i\omega_b t}+re^{-i\omega_b t}) & -i\kappa \end{pmatrix} \\ &=\sum_{n=-\infty}^{\infty} M^{(n)}e^{in\omega_b t}, \end{aligned} \tag{B.5}$$

where the last expression is the Fourier expansion of $M(t)$ and the Fourier components are defined as follows:

$$M^{(0)}=\begin{pmatrix} -\Xi-i\frac{\kappa}{2} & & \\ & \Xi-i\frac{\kappa}{2} & \\ & & -i\kappa \end{pmatrix}, \tag{B.6}$$

$$M^{(-1)}=\begin{pmatrix} 0 & 0 & \frac{\Omega}{2} \\ 0 & 0 & -r\frac{\Omega}{2} \\ \Omega & -r\Omega & 0 \end{pmatrix}, \tag{B.7}$$

$$M^{(+1)}=\begin{pmatrix} 0 & 0 & r\frac{\Omega}{2} \\ 0 & 0 & -\frac{\Omega}{2} \\ r\Omega & -\Omega & 0 \end{pmatrix}, \tag{B.8}$$

and $M^{(n)}$ is the 3×3 zero matrix when $n\neq 0,\pm 1$.

Assuming that

$$i\frac{d}{dt}\Pi(t,t')=M(t)\Pi(t,t'), \tag{B.9}$$

with $\Pi(t',t')=I_3$ and I_3 being a 3×3 identity matrix, the solution to the inhomogeneous equation can be found as

$$\vec{\sigma}(t) = \Pi(t,\, t')\vec{\sigma}(t') - \mathrm{i}\int_{t'}^{t} \Pi(t,\, s)\vec{\mathrm{b}}\mathrm{d}s. \tag{B.10}$$

The key task is to derive $\Pi(t,\, t')$, i.e. the principal matrix solution of the homogeneous part, which is assumed to take the following form in accordance to the Floquet theory [77, 79],

$$\Pi(t,\, t') = \sum_{j=1}^{3} |\phi_j(t)\rangle \langle\varphi_j(t')|\mathrm{e}^{-\mathrm{i}\lambda_j(t-t')}, \tag{B.11}$$

where $|\phi_j(t)\rangle = |\phi_j(t+T)\rangle$ is a 3×1 vector and $\langle\varphi_j(t')| = \langle\varphi_j(t'+T)|$ is a 1×3 vector. λ_j is a complex-valued exponent. It follows from equation (B.9) that

$$[M(t) - \mathrm{i}\partial_t]|\phi_j(t)\rangle = \lambda_j|\phi_j(t)\rangle, \tag{B.12}$$

$$[M^{\dagger}(t) - \mathrm{i}\partial_t]|\varphi_j(t)\rangle = \lambda_j^{*}|\varphi_j(t)\rangle. \tag{B.13}$$

The above differential equations can be solved by using the Fourier expansions:

$$|\phi_j(t)\rangle = \sum_{n=-\infty}^{\infty} |\phi_j^{(n)}\rangle \mathrm{e}^{\mathrm{i}n\omega_b t}, \tag{B.14}$$

$$|\varphi_j(t)\rangle = \sum_{n=-\infty}^{\infty} |\varphi_j^{(n)}\rangle \mathrm{e}^{\mathrm{i}n\omega_b t}, \tag{B.15}$$

where $|\phi_j^{n}\rangle$ and $|\varphi_j^{(n)}\rangle$ are the nth Fourier component of $|\phi_j(t)\rangle$ and $|\varphi_j(t)\rangle$, respectively. Substituting the expansions in equations (B.12) and (B.13), the differential equations are then converted into linear algebra equations

$$\sum_{k=-\infty}^{\infty} [M^{(n-k)} + n\omega_b I_3 \delta_{n,k}]|\phi_j^{(k)}\rangle = \lambda_j|\phi_j^{(n)}\rangle, \tag{B.16}$$

$$\sum_{k=-\infty}^{\infty} [M^{(k-n)} + n\omega_b I_3 \delta_{n,k}]^{\dagger}|\varphi_j^{(k)}\rangle = \lambda_j^{*}|\varphi_j^{(n)}\rangle, \tag{B.17}$$

which correspond to an eigenvalue problem of a nonHermitian matrix, i.e. $\mathcal{M}|\phi_j\rangle = \lambda_j|\phi_j\rangle$ and $\mathcal{M}^{\dagger}|\varphi_j\rangle = \lambda_j^{*}|\varphi_j\rangle$, where $|\phi_j\rangle$ and $|\varphi_j\rangle$ are the right and left eigenvectors, respectively, and $\mathcal{M}$ is consisting of infinite numbers of submatrices defined in the brackets and reads

$$\mathcal{M} = \sum_{n,k=-\infty}^{\infty}\sum_{j,j'=1}^{3} [M_{jj'}^{(n-k)} + k\omega_b\delta_{j,j'}\delta_{n,k}]\,|j,\, n\rangle\langle j',\, k|, \tag{B.18}$$

where $|j,\, n\rangle \equiv |j\rangle\otimes|n\rangle$, $\{|j\rangle|j=1,2,3\}$ is a set of orthonormal bases for 3-dimensional linear space, and $\{|n\rangle|n\in\mathbb{Z}\}$ is a set of orthonormal bases for infinite-dimensional linear space. The elements of the principal matrix solution can then be expressed in terms of the eigenvalues and eigenvectors of $\mathcal{M}$ as follows [77, 79]:

$$\begin{aligned}\Pi_{jj'}(t,\, t') &= \sum_{k,n=-\infty}^{\infty}\sum_{j''=1}^{3} \mathrm{e}^{\mathrm{i}k\omega_b t}\langle j,\, k|\phi_{j''n}\rangle \mathrm{e}^{-\mathrm{i}\lambda_{j''n}(t-t')}\langle\varphi_{j''n}|j',\, 0\rangle \\ &= \sum_{k=-\infty}^{\infty} \mathrm{e}^{\mathrm{i}k\omega_b t}\langle j,\, k|\mathrm{e}^{-\mathrm{i}\mathcal{M}(t-t')}|j',\, 0\rangle,\end{aligned} \tag{B.19}$$

where

$$\lambda_{j''n} \equiv \lambda_{j''} + n\omega_b, \tag{B.20}$$

and $|\phi_{j''n}\rangle$ and $\langle\varphi_{j''n}|$ are the corresponding right and left eigenvectors, respectively. In practice, one numerically diagonalize $\mathcal{M}$ to obtain its eigenvalues and eigenvectors with a truncation.

With $\Pi(t,\, t')$ at hand, we can easily calculate the single-time expectation. Particularly, in the the steady-state limit, we have

$$\begin{aligned}\langle\sigma_j(t)\rangle &= -\kappa\int_0^t \Pi_{j3}(t,\, s)\mathrm{d}s = -\sum_{l=-\infty}^{\infty} \mathrm{e}^{\mathrm{i}l\omega_b t}\langle j,\, l|\frac{\kappa}{\mathrm{i}\mathcal{M}}|3,\, 0\rangle \\ &\equiv \sum_{l=-\infty}^{\infty} \langle\sigma_j\rangle_{\mathrm{ss}}^{(l)}\mathrm{e}^{\mathrm{i}l\omega_b t} \quad (t\to\infty),\end{aligned} \tag{B.21}$$

where $j=1,2,3$ correspond to $\mu = +, -, z$, respectively. The two-time correlation function can be obtained from the single-time expectation by the quantum regression theorem [81], which reads

$$\langle\sigma_+(t)\sigma_-(t')\rangle = \Pi_{11}(t,\,t')\langle\sigma_+(t')\sigma_-(t')\rangle - \Pi_{13}(t,\,t')\langle\sigma_-(t')\rangle - \kappa\langle\sigma_-(t')\rangle\int_{t'}^{t}\Pi_{13}(t,\,s)\mathrm{d}s. \tag{B.22}$$

Letting $t = t' + \tau$ and $t' \to \infty$, we can derive a τ-dependent two-time correlation function in the steady-state limit,

$$\begin{aligned} g(\tau) &= \frac{1}{T}\int_0^T \lim_{t'\to\infty}\langle\sigma_+(t'+\tau)\sigma_-(t')\rangle\,dt' \\ &= \sum_{l=-\infty}^{\infty} \mathrm{e}^{\mathrm{i}l\omega_b\tau}\langle\sigma_+\rangle_{\mathrm{ss}}^{(l)}\langle\sigma_-\rangle_{\mathrm{ss}}^{(-l)} - \sum_{l=-\infty}^{\infty}\mathrm{e}^{\mathrm{i}l\omega_b\tau}\langle 1,\,l|\left(1-\frac{\kappa}{\mathrm{i}\mathcal{M}}\right)\mathrm{e}^{-\mathrm{i}\mathcal{M}\tau}|3,\,0\rangle\langle\sigma_-\rangle_{\mathrm{ss}}^{(-l)} \\ &\quad + \frac{1}{2}\sum_{l=-\infty}^{\infty}\mathrm{e}^{\mathrm{i}l\omega_b\tau}\langle 1,\,l|\mathrm{e}^{-\mathrm{i}\mathcal{M}\tau}|1,\,0\rangle[\delta_{l,0} + \langle\sigma_z\rangle_{\mathrm{ss}}^{(-l)}]. \end{aligned} \tag{B.23}$$

The Fourier transform of $g(\tau)$ leads to the formal spectrum

$$\begin{aligned} S(\Delta) = \sum_{l=-\infty}^{\infty}\pi|\langle\sigma_+\rangle_{\mathrm{ss}}^{(l)}|^2\delta(\Delta - l\omega_b) + \mathrm{Re}\sum_{l=-\infty}^{\infty}\Bigg\{\frac{1}{2}\langle 1,\,0|\frac{1}{\mathrm{i}(\mathcal{M}+\Delta I_\infty)}|1,\,l\rangle[\delta_{l,0}+\langle\sigma_z\rangle_{\mathrm{ss}}^{(l)}] \\ - \langle 1,\,0|\left(1-\frac{\kappa}{\mathrm{i}(\mathcal{M}-l\omega_b I_\infty)}\right)\frac{1}{\mathrm{i}(\mathcal{M}+\Delta I_\infty)}|3,\,l\rangle\langle\sigma_-\rangle_{\mathrm{ss}}^{(l)}\Bigg\}, \end{aligned} \tag{B.24}$$

where I_∞ is an infinite identity matrix. The spectral components consisting of the Dirac-delta functions are the coherent part of the fluorescence spectrum while the second summation in equation (B.24) gives rise to the incoherent part.

ORCID iDs

Yiying Yan https://orcid.org/0000-0003-4396-7265
Zhiguo Lü https://orcid.org/0000-0003-3560-4632

References

[1] Mollow B R 1969 *Phys. Rev.* **188** 1969–75
[2] Browne D E and Keitel C H 2000 *J. Mod. Opt.* **47** 1307–37
[3] Saiko A P, Markevich S A and Fedaruk R 2018 *JETP Lett.* **107** 129–33
[4] Narducci L M, Scully M O, Oppo G L, Ru P and Tredicce J R 1990 *Phys. Rev.* A **42** 1630–49
[5] Vogel W and Blatt R 1992 *Phys. Rev.* A **45** 3319–28
[6] Gao S Y, Li F L and Zhu S Y 2005 *Phys. Lett.* A **335** 110–20
[7] Macovei M, Evers J and Keitel C H 2005 *Phys. Rev.* A **71** 033802
[8] Wu J H, Li A J, Ding Y, Zhao Y C and Gao J Y 2005 *Phys. Rev.* A **72** 023802
[9] Antón M A, Calderón O G and Carreño F 2005 *Phys. Rev.* A **72** 023809
[10] Evers J, Bullock D and Keitel C H 2002 *Opt. Commun.* **209** 173–9
[11] Paspalakis E and Knight P L 1998 *Phys. Rev. Lett.* **81** 293–6
[12] Li A J, Song X L, Wei X G, Wang L and Gao J Y 2008 *Phys. Rev.* A **77** 053806
[13] Schmid S I and Evers J 2010 *Phys. Rev.* A **81** 063805
[14] Evers J, Kiffner M, Macovei M and Keitel C H 2006 *Phys. Rev.* A **73** 023804
[15] Macovei M, Evers J and Keitel C H 2003 *Phys. Rev. Lett.* **91** 233601
[16] Wang C L, Kang Z H, Tian S C, Jiang Y and Gao J Y 2009 *Phys. Rev.* A **79** 043810
[17] Carreño F, Antón M A, Yannopapas V and Paspalakis E 2017 *Phys. Rev.* A **95** 043825
[18] Gasparinetti S, Besse J C, Pechal M, Buijs R D, Eichler C, Carmichael H J and Wallraff A 2019 *Phys. Rev.* A **100** 033802
[19] Buffa R, Cavalieri S, Fini L and Matera M 1988 *J. Phys.* B **21** 239–47
[20] Janowicz M 1991 *Phys. Rev.* A **44** 3144–51
[21] Wilkens M and Rzążewski K 1989 *Phys. Rev.* A **40** 3164–78
[22] Paspalakis E, Keitel C H and Knight P L 1998 *Phys. Rev.* A **58** 4868–77
[23] Konthasinghe K, Peiris M and Muller A 2014 *Phys. Rev.* A **90** 023810
[24] Antón M A, Maede-Razavi S, Carreño F, Thanopulos I and Paspalakis E 2017 *Phys. Rev.* A **96** 063812
[25] Kryuchkyan G Y, Shahnazaryan V, Kibis O V and Shelykh I A 2017 *Phys. Rev.* A **95** 013834
[26] Gustin C, Manson R and Hughes S 2018 *Opt. Lett.* **43** 779
[27] Mohammadzadeh A and Miri M 2019 *Phys. Rev.* B **99** 115440
[28] Carmichael H J, Lane A S and Walls D F 1987 *Phys. Rev. Lett.* **58** 2539–42
[29] Freedhoff H and Quang T 1993 *J. Opt. Soc. Am.* B **10** 1337
[30] Rice P R and Pedrotti L M 1992 *J. Opt. Soc. Am.* B **9** 2008
[31] Cirac J I 1992 *Phys. Rev.* A **46** 4354–62
[32] Walls D F and Zoller P 1981 *Phys. Rev. Lett.* **47** 709–11
[33] Collett M, Walls D and Zoller P 1984 *Opt. Commun.* **52** 145–9
[34] Li F l, Gao S y and Zhu S y 2003 *Phys. Rev.* A **67** 063818
[35] Ficek Z, Dalton B J and Knight P L 1994 *Phys. Rev.* A **50** 2594–8
[36] Zhou P and Swain S 1999 *Phys. Rev.* A **59** 841–7

[37] Zhou P and Swain S 1999 *Phys. Rev.* A **59** 1603–7
[38] Jakob M and Kryuchkyan G Y 1998 *Phys. Rev.* A **58** 767–70
[39] Ficek Z and Swain S 1997 *J. Opt. Soc. Am.* B **14** 258
[40] Ficek Z, Dalton B J and Knight P L 1995 *Phys. Rev.* A **51** 4062–77
[41] Dalton B J, Ficek Z and Knight P L 1994 *Phys. Rev.* A **50** 2646–66
[42] Vogel W 1991 *Phys. Rev. Lett.* **67** 2450–2
[43] Gonzalo I, Antón M A, Carreño F and Calderón O G 2005 *Phys. Rev.* A **72** 033809
[44] Gao S Y, Li F L and Cai D L 2007 *J. Phys.* B **40** 3893–907
[45] Pegg D T, Loudon R and Knight P L 1986 *Phys. Rev.* A **33** 4085–91
[46] Huang H, Zhu S Y, Zubairy M S and Scully M O 1996 *Phys. Rev.* A **53** 1834–8
[47] Yang Y P, Xu J P, Chen H and Zhu S Y 2008 *Phys. Rev. Lett.* **100** 043601
[48] Kiffner M, Evers J and Keitel C H 2006 *Phys. Rev. Lett.* **96** 100403
[49] Kiffner M, Evers J and Keitel C H 2006 *Phys. Rev.* A **73** 063814
[50] Gao S Y, Li F L and Zhu S Y 2002 *Phys. Rev.* A **66** 043806
[51] Swain S, Zhou P and Ficek Z 2000 *Phys. Rev.* A **61** 043410
[52] Georgiades N, Polzik E and Kimble H 1999 *Phys. Rev.* A **59** 676–90
[53] Cardimona D A, Raymer M G and Stroud C R 1982 *J. Phys.* B **15** 55–64
[54] Norris D G, Orozco L A, Barberis-Blostein P and Carmichael H J 2010 *Phys. Rev. Lett.* **105** 123602
[55] Al-Khuzheyri R *et al* 2016 *Appl. Phys. Lett.* **109** 163104
[56] Dusanowski Ł, Kwon S H, Schneider C and Höfling S 2019 *Phys. Rev. Lett.* **122** 173602
[57] Kryuchkyan G Y, Jakob M and Sargsian A S 1998 *Phys. Rev.* A **57** 2091–5
[58] Strandberg I, Lu Y, Quijandría F and Johansson G 2019 *Phys. Rev.* A **100** 063808
[59] Hanschke L *et al* 2020 *Phys. Rev. Lett.* **125** 170402
[60] Wu F Y, Grove R E and Ezekiel S 1975 *Phys. Rev. Lett.* **35** 1426–9
[61] Ortiz-Gutiérrez L, Teixeira R C, Eloy A, da Silva D F, Kaiser R, Bachelard R and Fouché M 2019 *New J. Phys.* **21** 093019
[62] Ulrich S M, Ates S, Reitzenstein S, Löffler A, Forchel A and Michler P 2011 *Phys. Rev. Lett.* **106** 247402
[63] Ulhaq A, Weiler S, Roy C, Ulrich S M, Jetter M, Hughes S and Michler P 2013 *Opt. Express* **21** 4382
[64] Astafiev O, Zagoskin A M, Abdumalikov A A, Pashkin Y A, Yamamoto T, Inomata K, Nakamura Y and Tsai J S 2010 *Science* **327** 840–3
[65] Cohen-Tannoudji C and Reynaud S 1977 *J. Phys.* B **10** 345–63
[66] Cohen-Tannoudji C, Dupont-Roc J and Grynberg G 2004 *Atom-Photon Interactions: Basic Processes and Applications* (Weinheim: Wiley-VCH)
[67] Zhu Y, Wu Q, Lezama A, Gauthier D J and Mossberg T W 1990 *Phys. Rev.* A **41** 6574–6
[68] Freedhoff H and Chen Z 1990 *Phys. Rev.* A **41** 6013–22
[69] Agarwal G S, Zhu Y, Gauthier D J and Mossberg T W 1991 *J. Opt. Soc. Am.* B **8** 1163
[70] Ficek Z and Freedhoff H S 1993 *Phys. Rev.* A **48** 3092–104
[71] Ficek Z and Freedhoff H S 1996 *Phys. Rev.* A **53** 4275–87
[72] Yu C C, Bochinski J R, Kordich T M V, Mossberg T W and Ficek Z 1997 *Phys. Rev.* A **56** R4381–4
[73] Peiris M, Konthasinghe K, Yu Y, Niu Z C and Muller A 2014 *Phys. Rev.* B **89** 155305
[74] He Y *et al* 2015 *Phys. Rev. Lett.* **114** 097402
[75] Freedhoff H S and Ficek Z 1997 *Phys. Rev.* A **55** 1234–8
[76] Ruyten W M 1989 *Phys. Rev.* A **40** 1447–55
[77] Ho T S, Wang K and Chu S I 1986 *Phys. Rev.* A **33** 1798–816
[78] Yan Y, Lü Z and Zheng H 2016 *Ann. Phys.* **371** 159–82
[79] Shirley J H 1965 *Phys. Rev.* **138** B979–87
[80] Sambe H 1973 *Phys. Rev.* A **7** 2203–13
[81] Scully M O and Zubairy M S 1997 *Quantum Optics* (Cambridge: Cambridge University Press)
[82] Yan Y, Lü Z, Luo J and Zheng H 2019 *Phys. Rev.* A **100** 013823
[83] Geng X x, Jin K, Tang W w, Liang S, Yang G, Wu S p, Huang G m and Li G x 2022 *Phys. Rev.* A **106** 023108
[84] Geng X x, Yang G, Jin K, Tang W, Wu S p, Huang G m and Li G x 2022 *Laser & Photonics Reviews* **16** 2100614
[85] Breuer H P and Petruccione F 1997 *Phys. Rev.* A **55** 3101–16
[86] Yan Y L 2023 Github repository, bichromatic-field-RFspectra https://github.com/YiYYan/bichromatic-field-RFspectra